Geometrical optics in correlated imaging systems

De-Zhong Cao,[1] Jun Xiong,[1] and Kaige Wang[2,1,*]
[1]*Department of Physics, Applied Optics Beijing Area Major Laboratory, Beijing Normal University, Beijing 100875, China*
[2]*CCAST (World Laboratory), P.O. Box 8730, Beijing 100080, China*
(Received 30 June 2004; published 3 January 2005)

We discuss the geometrical optics of correlated imaging for two kinds of spatial correlations corresponding, respectively, to a classical thermal light source and a quantum two-photon entangled source. Due to the different features in the second-order spatial correlation, the two sources obey different imaging equations. The quantum entangled source behaves as a mirror, whereas the classical thermal source looks like a phase-conjugate mirror in the correlated imaging.

DOI: 10.1103/PhysRevA.71.013801 PACS number(s): 42.50.Dv, 42.30.Va, 42.65.Lm

An imaging method called coincidence imaging (correlated imaging or ghost imaging) has drawn much attention recently [1–11]. In this imaging system, the object and image are separately illuminated by a pair of correlated beams, and the image emerges through coincidence detection of the two beams. The first coincidence imaging experiments were carried out using a pair of entangled photons generated in spontaneous parametric down-conversion (SPDC) [1–3]. Recently, Gatti *et al.* [6] found that the ghost imaging can persist in high-gain SPDC, in which two entangled beams contain a large number of photons. Later on, in their further study appearing in [10], they proposed that the classical correlation of two beams obtained by splitting incoherent thermal radiation can perform the ghost imaging. However, the subwavelength interference effect, which was also regarded as a nonclassical effect related to two-photon entanglement, may have a classical counterpart with a thermal light source [10,12,13].

In this paper we focus on the geometrical optics of ghost imaging for both an entangled photon pair and a classical thermal light source. We find that the correlated imaging exhibits distinct aspects that cannot be included in ordinary imaging. However, the difference in spatial correlation between the quantum and classical sources is also reflected in the geometrical optics. In the SPDC of a type-I crystal, the down-converted beams contain both the quantum entanglement and the classical thermal correlation. When the crystal is used as a source, it can form a special dual correlation imaging system, in which an object can simultaneously produce two correlated images. The system may find potential application in optical design.

We consider classical thermal light described by $E(\mathbf{x},z,t)=\int E(\mathbf{q})\exp[i\mathbf{q}\cdot\mathbf{x}]d\mathbf{q}\,\exp[i(kz-\omega t)]$, in which $E(\mathbf{q})$ is a stochastic variable obeying Gaussian statistics and $\mathbf{q}$ is the transverse wave vector satisfying $|\mathbf{q}|\ll k$. For any thermal statistics, the second-order spectral correlation is written as

$$\begin{aligned}&\langle E^*(\mathbf{q}_1)E^*(\mathbf{q}_2)E(\mathbf{q}_2')E(\mathbf{q}_1')\rangle\\&\quad=\langle E^*(\mathbf{q}_1)E(\mathbf{q}_1')\rangle\langle E^*(\mathbf{q}_2)E(\mathbf{q}_2')\rangle\\&\qquad+\langle E^*(\mathbf{q}_1)E(\mathbf{q}_2')\rangle\langle E^*(\mathbf{q}_2)E(\mathbf{q}_1')\rangle=S(\mathbf{q}_1)S(\mathbf{q}_2)\\&\qquad\times[\delta(\mathbf{q}_1-\mathbf{q}_1')\delta(\mathbf{q}_2-\mathbf{q}_2')+\delta(\mathbf{q}_1-\mathbf{q}_2')\delta(\mathbf{q}_2-\mathbf{q}_1')],\end{aligned}\quad(1)$$

where $S(\mathbf{q})$ is the power spectrum of the spatial frequency. For comparison, we show the second-order correlation of the entangled beams generated in the lower gain limit of SPDC [13],

$$\begin{aligned}&\langle a_m^\dagger(\mathbf{q}_1)a_n^\dagger(\mathbf{q}_2)a_n(\mathbf{q}_2')a_m(\mathbf{q}_1')\rangle\\&\quad=W^*(\mathbf{q}_1)W(\mathbf{q}_1')\delta(\mathbf{q}_1+\mathbf{q}_2)\delta(\mathbf{q}_1'+\mathbf{q}_2'),\end{aligned}\quad(2)$$

where the subscripts m and n indicate the polarizations of the beams for a type-II crystal. The spectrum $W(\mathbf{q})$ depends on the transfer functions of SPDC. The equation is also valid for a type-I crystal, in which the down-converted beams have the same polarization, and the subscripts m and n can be omitted. Therefore, both the thermal light and the entangled photon pair exhibit transverse wave vector correlation. The former shows the self-correlation of transverse wave vectors between positive and negative components, while the latter shows the correlation of a pair of conjugate wave vectors satisfying the momentum conservation, within the same spatial frequency component.

To show correlated imaging of thermal light, we may use a 50-50 beam splitter which divides the input beam into two correlated beams. For the sake of comparison with the thermal light, we assume central-frequency degeneracy for the two-entangled-photon source. Furthermore, the beam splitter is also applied to the quantum imaging system. This corresponds to the collinear case of SPDC, where the entangled down-converted photons are spatially divided by a beam splitter for the coincidence imaging. However, for a type-II phase-matching configuration, the down-converted beam is divided by a polarization beam splitter [2]. We define $F_i(\mathbf{q})$ $(i=1,2)$ as the two output fields of the beam splitter. For both classical and quantum sources, the second-order correlation of the output fields $\langle F_1^*(\mathbf{q}_1)F_1(\mathbf{q}_1')F_2^*(\mathbf{q}_2)F_2(\mathbf{q}_2')\rangle$ is proportional to that of the input, i.e., Eqs. (1) and (2). For simplicity, we consider the one-dimensional case. Let $h_i(x,x')$ $(i=1,2)$ be the impulse response function for the i path in the correlated imaging scheme, then the joint intensity at the two detective planes is obtained to be

$$\begin{aligned}&\langle I_1(x_1)I_2(x_2)\rangle\\&\quad=\int h_1^*(x_1,-q_1)h_1(x_1,-q_1')h_2^*(x_2,-q_2)h_2(x_2,-q_2')\\&\qquad\times\langle F_1^*(q_1)F_1(q_1')F_2^*(q_2)F_2(q_2')\rangle dq_1dq_1'dq_2dq_2',\end{aligned}\quad(3)$$

*Corresponding author: wangkg@bnu.edu.cn

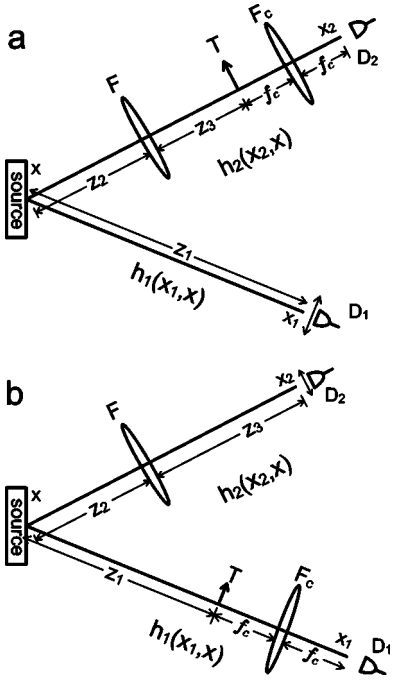

FIG. 1. Sketches of correlated imaging for (a) scheme I, where object T and the imaging lens F are in the same path and (b) scheme II, where T and F are in different paths. F_c is the collective lens so that the object and the detector are placed in its two focal planes.

where $h_i(x,q)=(1/\sqrt{2\pi})\int h_i(x,x')\exp(-iqx')dx'$. Substituting Eqs. (1) and (2) into Eq. (3), we obtain the joint intensity

$$\langle I_1(x_1)I_2(x_2)\rangle \propto \int S(q)|h_1(x_1,-q)|^2dq \int S(q)|h_2(x_2,-q)|^2dq + \left|\int S(q)h_1^*(x_1,-q)h_2(x_2,-q)dq\right|^2, \quad (4a)$$

$$\langle I_1(x_1)I_2(x_2)\rangle \propto \left|\int W(q)h_1(x_1,-q)h_2(x_2,q)dq\right|^2, \quad (4b)$$

for the classical and quantum sources, respectively. These results are identical to those in Ref. [10] in which the joint intensity correlations are evaluated by the impulse functions $h_i(x,x')$ instead of $h_i(x,q)$. Equations (4) show macroscopically the difference between the classical and quantum correlated imaging. For the thermal source, the first term of Eq. (4a) reflects the background while the second term expresses the correlated imaging. Therefore, the classical correlated imaging has lower visibility than the quantum one. Furthermore, the nature of the wave vector correlations for the classical and quantum sources is also reflected in the correlations of the two impulse response functions. This will result in different imaging laws.

Now we discuss the two schemes of correlated imaging as shown in Fig. 1. For simplicity, we assume that the beam splitter is close to the source, so that the beam is divided immediately from the source [14]. For scheme I, the two impulse response functions are written as

$$h_1(x_1,q)=(1/\sqrt{2\pi})\exp\left(ikz_1-iqx_1-i\frac{q^2z_1}{2k}\right), \quad (5a)$$

$$h_2(x_2,q)=\frac{1}{2\pi}\sqrt{\frac{kf}{i(f-z_3)f_c}}\exp\left[ik(z_2+z_3+2f_c) - i\frac{q^2}{2k}\left(z_2+\frac{z_3f}{f-z_3}\right)\right] \times\int T(x)\exp\left[i\frac{kx^2}{2(z_3-f)} - i\left(\frac{kx_2}{f_c}+\frac{qf}{f-z_3}\right)x\right]dx \quad (z_3\neq f), \quad (5b)$$

$$h_2(x_2,q)=\frac{1}{2\pi i}\sqrt{\frac{f}{f_c}}\exp\left(ik(z_2+f+2f_c)+i\frac{q^2}{2k}(f-z_2) + i\frac{f}{f_c}x_2q\right)T\left(-\frac{qf}{k}\right) \quad (z_3=f),$$

where f and f_c are the focal lengths of the imaging lens F and the collective lens F_c, respectively, z_1 and z_2 are the distances from the source to detector D_1 and lens F, respectively, z_3 is the distance between object T and lens F, and $T(x)$ is the transmission function of object T. For scheme II, however, the two impulse response functions are written as

$$h_1(x_1,q)=\frac{1}{2\pi}\sqrt{\frac{k}{if_c}}\exp\left(ik(z_1+2f_c)-i\frac{z_1q^2}{2k}\right) \times\int T(x)\exp\left[-i\left(\frac{kx_1}{f_c}+q\right)x\right]dx, \quad (6a)$$

$$h_2(x_2,q)=\sqrt{\frac{f}{2\pi(f-z_3)}}\exp\left[ik(z_2+z_3)-i\frac{q^2}{2k}\left(z_2+\frac{z_3f}{f-z_3}\right) - i\frac{qx_2f}{f-z_3}-i\frac{kx_2^2}{2(f-z_3)}\right] \quad (z_3\neq f), \quad (6b)$$

$$h_2(x_2,q)=\sqrt{\frac{k}{2\pi if}}\exp\left(ik(z_2+f)+ik\frac{x_2^2}{2f^2}(f-z_2)\right) \times\delta\left(\frac{k}{f}x_2+q\right) \quad (z_3=f),$$

where z_1 and z_2 are the distances from the source to object T and the imaging lens F, respectively; z_3 is the distance between lens F and detector D_2. In the broadband limit, $W(q)$ and $S(q)$ can be regarded as a constant in the integration, and we calculate the joint intensity using Eq. (4). For both schemes, we introduce the correlated imaging equations

$$\frac{1}{z_2-z_1}+\frac{1}{z_3}=\frac{1}{f} \quad \text{for classical correlated imaging,} \quad (7a)$$

$$\frac{1}{z_2+z_1}+\frac{1}{z_3}=\frac{1}{f} \quad \text{for quantum correlated imaging,} \quad (7b)$$

under which the correlated imaging is obtained to be

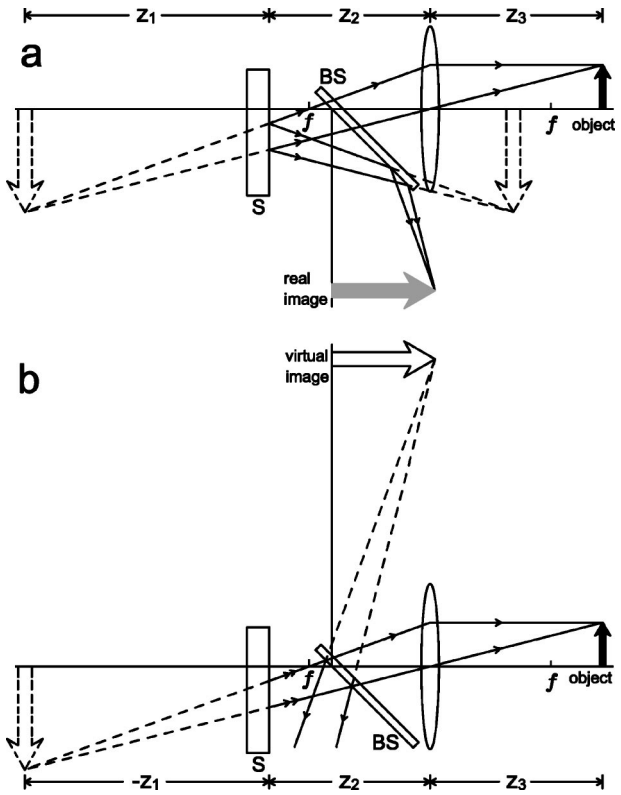

FIG. 2. Correlated imaging for scheme I in which $z_3 > f$ and the condition $z_3 f/(z_3 - f) - z_2 > 0$ are satisfied. (a) A real correlated image is formed for the source with quantum entanglement; (b) a virtual correlated image is formed for the source with thermal correlation. In Figs. 2–5 the objects, the real images, and the virtual images are indicated by dark, gray, and hollow arrows, respectively, and the intermediate images are indicated by dashed arrows.

$$\langle I_1(x_1) I_2(x_2) \rangle \sim \begin{cases} |T[x_1(f - z_3)/f]|^2 & \text{for scheme I,} \\ |T[x_2 f/(f - z_3)]|^2 & \text{for scheme II.} \end{cases} \quad (8)$$

Equation (7b) is known for the quantum coincidence imaging configured in scheme I [2], and we extend it now to scheme II. Note that Eq. (8) is valid for both the quantum and classical cases when the background term is removed for the classical case. The correlated imaging (8) is independent of position x_2 (x_1) of detector D_2 (D_1) for scheme I (II), since detector D_2 (D_1) and lens F_c form a collective detection. However, z_3 is the object distance for scheme I or the imaging distance for scheme II, so that Eq. (8) gives the same magnification as that in the ordinary imaging.

In the correlated imaging equations (7), the joint path $z_2 \pm z_1$ is the imaging distance for scheme I or the object distance for scheme II, reflecting the nature of the quantum and classical correlations. Although the correlated imaging equation is similar to the ordinary one, it will cause rich and even surprising imaging effects that cannot be covered by the ordinary imaging law; for example, a virtual image can become real, and vice versa. Let us discuss the two schemes in detail.

Scheme I. When the object distance is greater than the focal length $z_3 > f$, the joint path image distance $z_2 \pm z_1$ is positive. But this does not assure a real correlated image. Since z_2 is positive by definition, and z_1 could be either positive or negative, the former causes a real correlated image while the latter causes a virtual one. In the case $z_3 > f$, the condition for a real correlated image is $z_3 f/(z_3 - f) - z_2 > 0$ (< 0) for the source with quantum entanglement (classical thermal correlation). For the opposite condition, however, the correlated image is virtual. A virtual correlated image cannot be directly observed in the correlated detection.

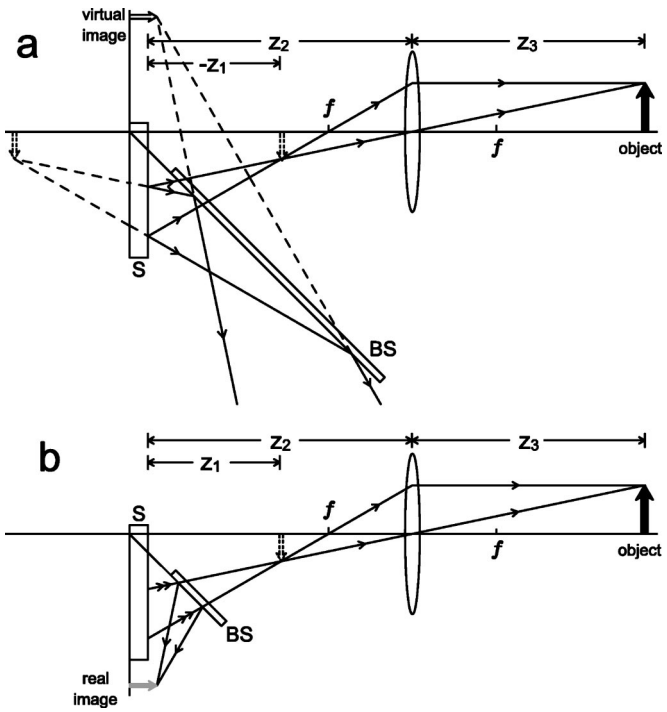

FIG. 3. Same as in Fig. 2 but the condition $z_3 f/(z_3 - f) - z_2 < 0$ is satisfied. (a) A virtual correlated image is formed for the source with quantum entanglement; (b) a real correlated image is formed for the source with thermal correlation.

Next we consider the case of the object distance less than the focal length $z_3 < f$, for which the joint path $z_2 \pm z_1$ as the image distance is negative. This means that z_1 is negative for the quantum coincidence imaging and positive for the classical correlated imaging; therefore, a virtual image in the ordinary imaging system becomes real in the classical correlated imaging.

The correlated imaging can be plotted by the graphics of ray optics, by taking into account the correlation of rays emitted from the source. We first plot the image in the ordinary way. Then, for the source with quantum entanglement, the image is reflected twice, first by the source and then by the beam splitter. Obviously, the beam splitter plays the role of a mirror. However, the quantum source emits a pair of correlated rays with opposite transverse wave vectors, one to the object and the other to the image, so that it also acts as a mirror. For the source with the thermal correlation, the image is reflected only by the beam splitter. This geometry is due to the nature of the self-correlation of the wave vectors, so that the thermal source acts as a phase-conjugate mirror and hence the image is reflected to itself. According to these rules, we plot the coincidence imaging for $z_3 > f$ in Figs. 2

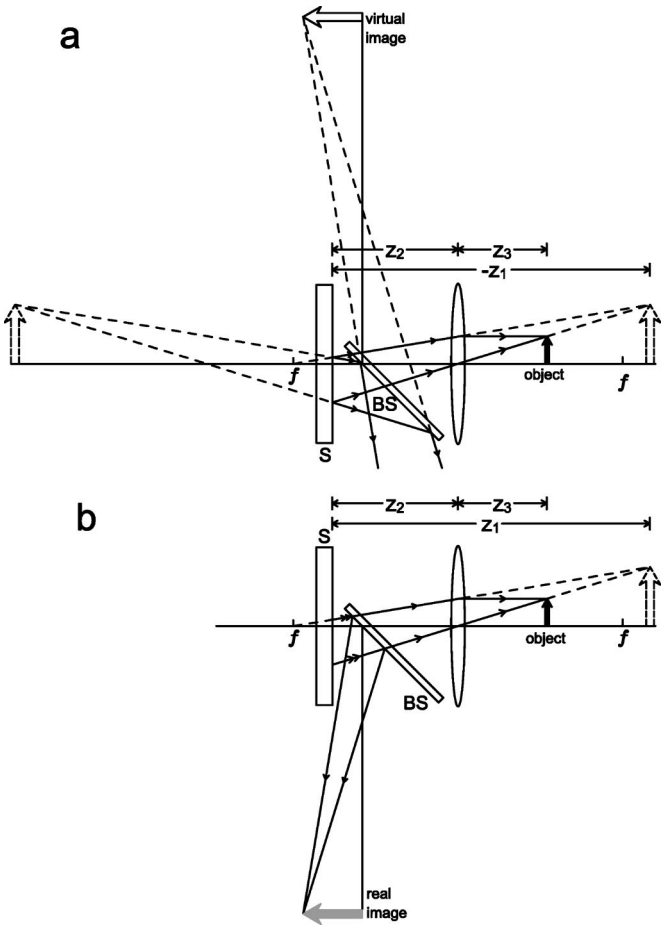

FIG. 4. Correlated imaging for scheme I in the case $z_3 < f$. (a) A virtual correlated image is formed for the source with quantum entanglement; (b) a real correlated image is formed for the source with thermal correlation.

and 3, and $z_3 < f$ in Fig. 4. For comparison, we arrange the same optical setup for the two sources: the quantum entanglement in Figs. 2(a), 3(a), and 4(a) and the classical thermal correlation in Figs. 2(b), 3(b), and 4(b). The negative image distances z_1 indicate the virtual images. These figures verify the above analysis: while the quantum coincidence image is virtual, the classical coincidence image must be real, or vice versa.

Scheme II. In this scheme, the joint path $z_2 \pm z_1$ is the object distance while z_3 is the image distance. Just as with the ordinary imaging law, when the joint path $z_2 \pm z_1$ is greater (less) than the focal length, the correlated image is real (virtual). Different from scheme I, for the same optical setup with different sources, the quantum and classical correlated images can be both real. In Fig. 5, we plot the two real correlated images for $z_2 \pm z_1 > f$. In the graphics of this scheme, we should move the object to the optical axes of the lens. For the source with the quantum entanglement, the object is reflected twice, first by the beam splitter and then by the source, as shown in Fig. 5(a). For the classical correlation, however, the object is reflected only by the beam splitter, as shown in Fig. 5(b).

It can be seen from Figs. 5 that, for the classical correlation source, a real correlated image can be formed through the beam splitter without using a lens. This fact is also included in the imaging equation by setting an infinite focal length for lens F. For the classical source, this results in $z_2 + z_3 = z_1 > 0$, and object and real imaging have an equal distance from the source. As indicated above, the classical thermal source behaves as a phase conjugate mirror which reflects an object to itself. This feature manifests the self correlation of the transverse wave vector for classical thermal light.

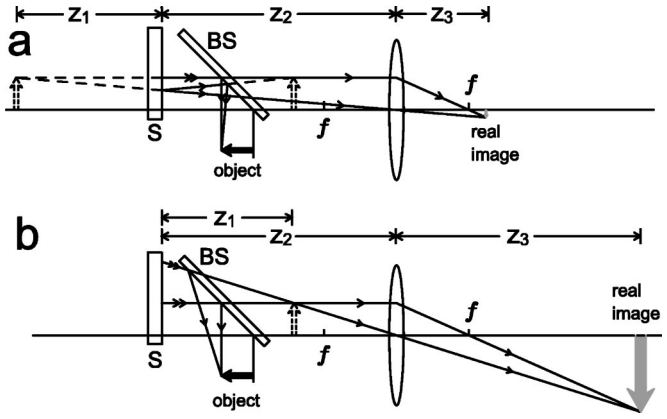

FIG. 5. Correlated imaging for scheme II in the case $z_2 \pm z_1 > f$. The real correlated images are formed for both the sources: (a) with quantum entanglement and (b) with thermal correlation.

Spatial thermal correlation (1) also exists in the SPDC process. In type-II SPDC, the quantum entanglement occurs between two beams with different polarizations. But if one beam with a particular polarization is extracted, it exhibits thermal correlation [13]. However, the beam generated in type-I SPDC may incorporate both quantum entanglement and classical thermal correlation [13]. When the gain of SPDC is lower, the proportion of the thermal correlation is lower than that of the quantum entanglement, i.e., $|S(q)| < |W(q)|$. In the case of strong SPDC coupling, $|S(q)|$ is increased and comparable with $|W(q)|$ [12]. Using this source, a dual correlated imaging system can be formed, in which two kinds of correlated imaging are created simultaneously. For scheme I, the classical correlated image is real while the quantum one must be virtual, and vice versa. For scheme II, however, the two images can be both real or both virtual, or one real and the other virtual, depending on the values of z_1 and z_2.

In summary, we have derived the correlated imaging equation for the classical thermal light source and have shown the macroscopic differences of quantum and classical correlated imaging. The unusual and rich correlated imaging effects may provide potential applications in optical designs.

The authors thank L. A. Wu for helpful discussions. This research was supported by the National Fundamental Research Program of China Project No. 2001CB309310, and the National Natural Science Foundation of China, Project Nos. 60278021, 10074008, and 10174007.

[1] D. V. Strekalov, A. V. Sergienko, D. N. Klyshko, and Y. H. Shih, Phys. Rev. Lett. **74**, 3600 (1995).
[2] T. B. Pittman, Y. H. Shih, D. V. Strekalov, and A. V. Sergienko, Phys. Rev. A **52**, R3429 (1995).
[3] P. H. S. Ribeiro, S. Pádua, J. C. Machado da Silva, and G. A. Barbosa, Phys. Rev. A **49**, 4176 (1994).
[4] B. E. A. Saleh, A. F. Abouraddy, A. V. Sergienko, and M. C. Teich, Phys. Rev. A **62**, 043816 (2000).
[5] A. F. Abouraddy, B. E. A. Saleh, A. V. Sergienko, and M. C. Teich, Phys. Rev. Lett. **87**, 123602 (2001); J. Opt. Soc. Am. B **19**, 1174 (2002).
[6] A. Gatti, E. Brambilla, and L. A. Lugiato, Phys. Rev. Lett. **90**, 133603 (2003).
[7] R. S. Bennink, S. J. Bentley, and R. W. Boyd, Phys. Rev. Lett. **89**, 113601 (2002); R. S. Bennink, S. J. Bentley, R. W. Boyd, and J. C. Howell, *ibid.* **92**, 033601 (2004).
[8] M. D'Angelo, Y.-H. Kim, S. P. Kulik, and Y. Shih, Phys. Rev. Lett. **92**, 233601 (2004).
[9] J. Cheng and Sh. Han, Phys. Rev. Lett. **92**, 093903 (2004).
[10] A. Gatti, E. Brambilla, M. Bache, and L. A. Lugiato, Phys. Rev. A **70**, 013802 (2004); Phys. Rev. Lett. **93**, 093602 (2004).
[11] Y. Cai and Sh-Y. Zhu, e-print quant-ph/0407240. (In this work, the authors obtained the same correlated imaging equation of thermal light.)
[12] D. Zh. Cao and K. Wang, Phys. Lett. A **333**, 23 (2004); D. Zh. Cao, Zh. Li, Y. H. Zhai, and K. Wang, e-print quant-ph/0401109.
[13] K. Wang and D. Zh. Cao, Phys. Rev. A **70**, 041801(R) (2004).
[14] Further theoretical analysis shows that this assumption is not necessary to obtain the imaging equations (7).